Enhancing Luminescence Efficiency by Controlled Island Formation of CsPbBr₃ Perovskite

Tobias Antrack,* Martin Kroll, Lena Merten, Miguel Albaladejo-Siguan,
Alexander Hinderhofer, Oleg V. Konovalov, Maciej Jankowski, Johannes Benduhn,
Frank Schreiber, Yana Vaynzof, and Karl Leo*

CsPbBr₃ is an inorganic perovskite material that is promising for light-emitting applications. Such applications are known to benefit from an island-type active layer structure, which enhances the device's light emission efficiency. Here, the impact of the environment on the island formation in thermally deposited bilayers of CsPbBr₃/LiBr is investigated. It is demonstrated that the island formation occurs only in humid environments, leading to an enhancement of the photoluminescence quantum yield by a factor of 350. Time-resolved grazing-incidence wide-angle X-ray scattering experiments document the island growth process and reveal that the LiBr has already changed the perovskite crystal orientation prior to the island formation.

1. Introduction

In recent years, perovskites have been of highest interest in the research of optoelectronic materials.[1] Intense investigations have led to large increases in the efficiency of both solar cells (power conversion efficiencies > 25%[2,3]) and light-emitting diodes (LEDs, external quantum efficiency > 20%).[4,5] These advances are made possible by the excellent optoelectronic properties of lead halide perovskites, particularly their high photoluminescence quantum yield (PLQY).[6,7] To reach higher efficiencies of perovskite-based LEDs, nonradiative recombination processes of the charge carriers need to be further suppressed.[8] Since excitons in lead halide perovskites often have a relatively small binding energy, they are very likely to dissociate in the bulk before radiative recombination occurs.[9] Consequently, several approaches have been developed to circumvent this process. For example, Xiao and co-workers demonstrated efficient perovskite LEDs by forming nanometer-sized crystallites within the active layer.[10] In such crystallites, the excitons are confined and thus are far less likely to dissociate prior to radiative recombination. More recently Dumont et al. reported a similar enhancement in the case of the formation of much larger, sub-micrometer sized islands.[11] The authors used contact-angle measurements and demonstrated that a transformation from a continuous thin film to islands can be achieved by depositing a thin layer of LiBr on top of CsPbBr₃, which changes the surface tension such that migration of material into clusters is occurring already at room temperature. Importantly, this method is applicable to thermally deposited perovskite layers, which is particularly promising for a potential future application on an industrial level, due to its many benefits in terms of scalability, homogeneity, and process control.[12]

In this work, we take a closer look at the crystal orientation and the process of perovskite migration into islands, particularly the crucial role of environmental factors in this process. To better understand the process, we use 2 nm thick LiBr layers on both the top and bottom of a 60 nm thick CsPbBr₃ perovskite layer. The perovskite layer and the LiBr layers are significantly thicker than in the work of Dumont et al. We observe a faster growth and larger islands as a result, which makes it easier to observe the mass transport. To avoid any influences of the glass substrate on the crystal formation and subsequent degradation, 5 nm of 1,3,5-tris(2-*N*-phenylbenzimidazolyl) benzene (TPBi) is first evaporated onto the substrate. Then, for passivation and symmetry purposes, 5 nm of TPBi is additionally evaporated on top of the structure.

T. Antrack, M. Kroll, M. Albaladejo-Siguan, J. Benduhn, Y. Vaynzof, K. Leo
Dresden Integrated Center for Applied Physics and Photonic Materials
(IAPP) and Institute of Applied Physics
Technische Universität Dresden
Nöthnitzer Str. 61, 01187 Dresden, Germany
E-mail: tobias.antrack@tu-dresden.de; karl.leo@tu-dresden.de
L. Merten, A. Hinderhofer, F. Schreiber
Institut für Angewandte Physik
Universität Tübingen
Auf der Morgenstelle 10, 72076 Tübingen, Germany
O. V. Konovalov, M. Jankowski
The European Synchrotron-ESRF
71 Avenue des Martyrs, CS 40220, Grenoble Cedex 9 38043, France

2. Results and Discussion

2.1. Strong Increase in PLQY

Considering that the vacuum chamber used for deposition of the investigated samples is located inside a nitrogen-filled
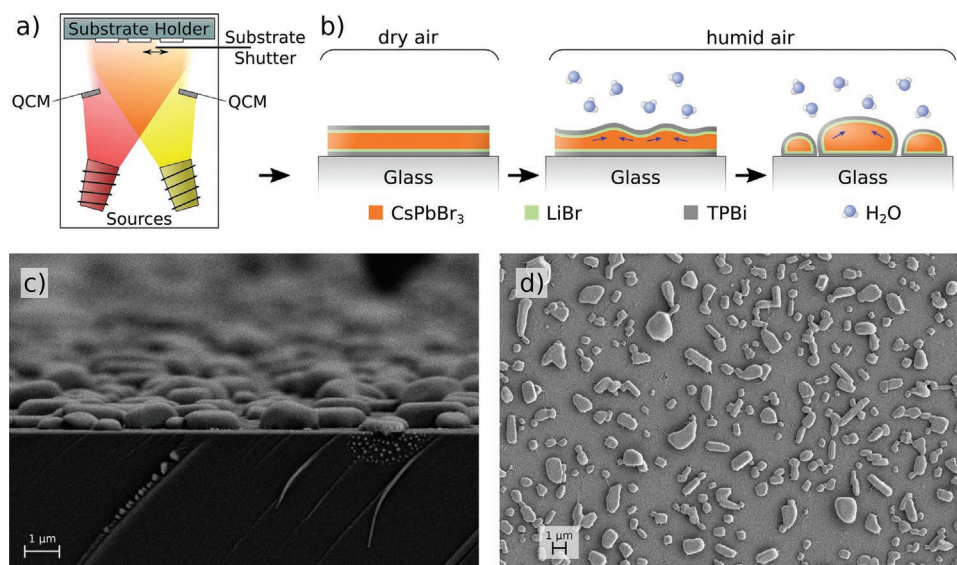
Figure 1. a) Sketch of the vacuum deposition and b) the island formation due to mass transport. c) Cross-sectional scanning electron microscope (SEM) image of islands (acquired with 2° inclination of the sample) and d) top-view of differently shaped islands with sizes varying from 0.6 to 2.2 µm.

glovebox, we were able to control the exposure to the environment of the fabricated samples. Upon fabrication and subsequent removal of the samples from the deposition chamber, the samples appeared shiny, which suggests they exhibit very smooth surfaces. However, once exposed to ambient air (≈25% relative humidity), the samples' appearance changed to be milky, suggesting significant light scattering by a starkly changed morphology (**Figure 1**b). To investigate this change's impact on the samples' optical properties, their PLQY was measured as a function of time upon exposure to ambient air (**Figure 2**a). First, we find that there is no change in emission intensity and spectrum as long as the integrating sphere is purged with nitrogen. But upon contact with ambient air, the emission efficiency of the samples is drastically increasing over 4.5 h, reaching its maximum value of 17.9%. Compared to the first measurement taken a few seconds after the first contact with ambient air, where a PLQY of 0.05% was obtained, this corresponds to an increase by a factor of ≈350. This is significantly larger than the increase of PLQY by a factor of 11 reported by Dumont et al. when adding a thin LiBr layer
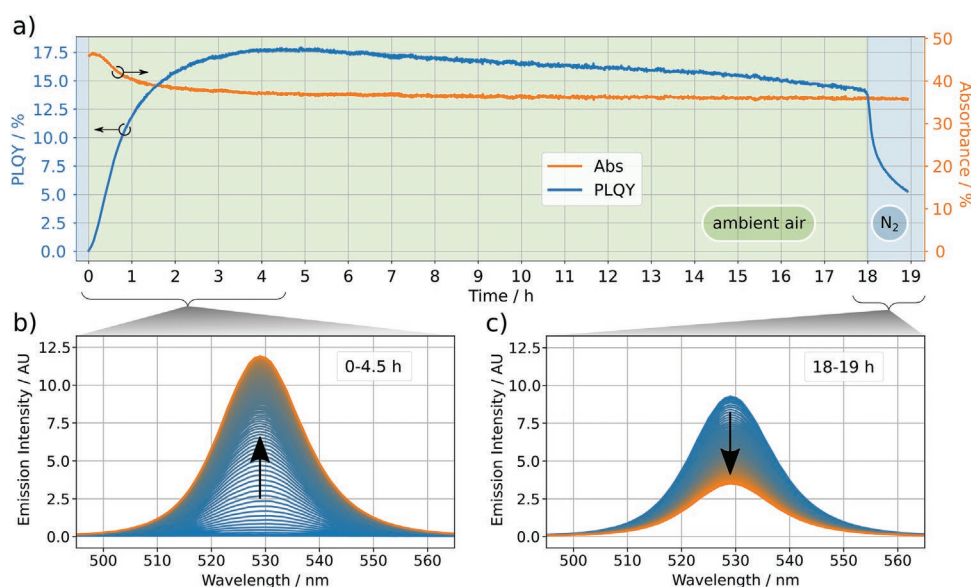

Figure 2. a) PLQY measurements and absorbance in ≈25% humidity during island formation of a fresh sample. After 4.5 h, a PLQY of 17.9% was measured, which is an increase of 350 times compared to the first measurement of 0.05% for a fresh sample with no contact to humidity. After 18 h, nitrogen flow into the integrating sphere is activated, drastically lowering emission efficiency. b) The emission spectra during the increase of PLQY (from 0 to 4.5 h, shown for every x min.) show no change in spectral shape and c) also no change is observed when the emission is decreased due to nitrogen flow (from 18 to 19 h).
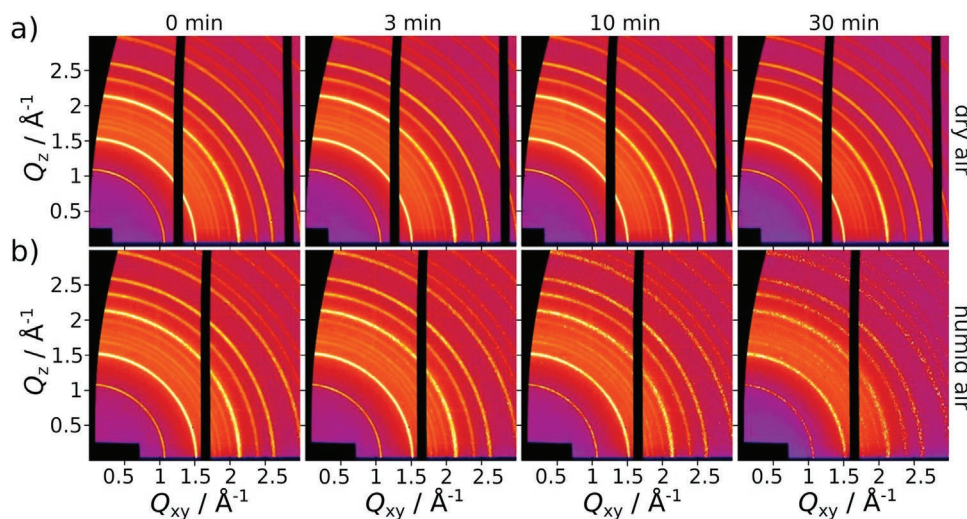
2201408 (2 of 5)

Figure 3. In situ GIWAXS measurements for different time steps (0, 3, 10, and 30 min) a) when the sample was exposed to dry air and b) when exposed to humid air. No notable changes are found when exposed to dry air, whereas the smooth rings turn grainy with increasing exposure time to humid air. The black areas are shadows of the beam-stop, inaccessible Q values in the given geometry, and gaps in the detector area.

compared to pure $CsPbBr_3$. The authors suggested that this increase is related to the positive impacts of the LiBr layer on the Cs/Pb chemical stoichiometry as well as a reduction of Br vacancies and a shift of the Fermi energy level toward the conduction band minimum.[11] On the other hand, Girolamo et al. have shown that humidity can positively affect the crystallinity of $CsPbBr_3$ when applied for a limited amount of time.[13] They reported an increase in the PLQY by up to a factor of 30 during exposure to a humidity of 60–80%. In our approach, where both LiBr and a humid environment are combined, the effects observed in these studies are expected to play a role.

Quantum confinement increases the overlapping of the charge carrier wave functions and therefore increases the radiative recombination probability. With island sizes varying between 0.6 and 2.2 µm (Figure 1c,d) and an exciton Bohr diameter of 7 nm,[14,15] we do not expect quantum confinement to be relevant. However, excitons are known to rapidly dissociate in bulk $CsPbBr_3$,[9] and by spatially confining the excitons, this process can be suppressed, which results in a higher PLQY.[11] In addition, the high surface roughness, compared to smooth layers, increases the outcoupling efficiency due to scattering and suppressed total internal reflection.[16,17]

After reaching its maximum, the PLQY slowly decreases with a rate of roughly 0.28% in absolute terms per hour. Here, nanoscale phase impurities could be seeds for photoinduced degradation of the perovskite material.[17] This process might be competing with island formation regarding PLQY. After 18 h, the integrating sphere was purged with nitrogen and the measurement was continued. This change in atmosphere results in a drastic drop in PLQY. It appears that a permanent presence of humidity is necessary to guarantee a certain PLQY, which could be explained by the positive effect of humidity on the perovskite crystallinity,[13] but the precise mechanisms are yet to be understood. A morphology transformation from islands back to a continuous film due to the absence of humidity is very unlikely since no mass transport was observed during scanning electron microscopy (SEM) measurements even after over 1 h

in high vacuum. Additionally, after months of storing samples with islands formed in nitrogen atmosphere, the surface still appears milky which indicates a high surface roughness due to island presence (Figure S6, Supporting Information). However, Guo et al. reported that degradation mechanisms can be different under nitrogen atmosphere and vacuum with light-induced phase segregation and morphology deformation only occurring in vacuum. Since we do not observe these effects in vacuum, it is unlikely they are playing a major role when the integrating sphere is purged with nitrogen.[18]

Neither during the increase of PLQY (Figure 2b) nor the slow decrease and the decrease due to nitrogen flow can a spectral change of the emission be observed (Figure 2c). Furthermore, a measurement after 2 months reveals a decrease in emission intensity of one order of magnitude but, again, no change in the emission spectrum, c.f. Figure S5 in the Supporting Information.

2.2. Crystal Orientation

To gain further insights into the island formation process, it was monitored in real-time using grazing incidence wide-angle X-ray scattering (GIWAXS)[18] to monitor structural changes upon air and humidity exposure. All fresh samples had a similar crystal structure and orientation, which is notably different from the one of a similar perovskite film without the presence of LiBr, as shown in Figure S4 in the Supporting Information. The mere presence of LiBr causes the material to grow with a tilted crystal orientation relative to the substrate instead of vertical orientation without LiBr. The average crystal orientation does not change significantly during exposure to air and humidity. However, the crystal size change is apparent from the change of smooth diffraction rings (**Figure 3**b, first image) to a grainier diffraction pattern (Figure 3b, last image), indicating scattering by fewer but larger grains. This change, however, only occurs when the sample is exposed to humid air.

**ADVANCED
SCIENCE NEWS**

www.advancedsciencenews.com

**ADVANCED
OPTICAL
MATERIALS**

www.advopticalmat.de

As shown in Figure 3a, during exposure to dry air, no significant changes are observed in the diffraction pattern even after 30 min of exposure. On the other hand, after a few minutes of treatment with humid air, a notable change can be observed. This finding clearly indicates that humidity is necessary to induce the growth of large islands.

Two important observations from the real-time GIWAXS data lead to a better understanding of the island formation process. First, the average domain orientation is unchanged during island formation. Second, the noncontinuous (grainy) appearance of the scattering rings indicates that the large grains have only one crystal orientation within each grain. With few to no grain boundaries visible on islands in the SEM images (Figure 1d and Figure S6, Supporting Information), it can be concluded that the islands consist of only one crystalline domain and, therefore, the observed increase in grain size represents the process of island formation.

The increase of grain size results in fewer grain boundaries and, therefore, fewer crystal defects that can facilitate nonradiative recombination.[19] This effect is expected to contribute to the observed increase of PLQY. To further improve the understanding of the process of island formation, the in situ observation of GIWAXS and PLQY could be done simultaneously in a specialized setup.[20]

2.3. Observation of Island Growth

With a final island size in the μm-range, even a light microscope is able to observe the growth process and images were taken every 5 s. In Figure S1 in the Supporting Information, it can be seen that small arbitrarily distributed islands are formed directly in the first moments of exposure to humidity. Within minutes, many new islands appear and grow in size until they eventually interconnect into larger islands. In Figure 1d, it can be seen that some of the larger islands have formed by connecting smaller islands. During the entire observation time of 90 min, the islands continuously grew, which fits the continuous increase of PLQY in Figure 2a. After one day, the islands are more isolated and larger, with sizes of up to 3 μm. This continuous increase in size explains the decrease in PLQY after about 4.5 h in Figure 2a because the spatial confinement of excitons gets less relevant and dissociation becomes more likely.[11]

SEM measurements on fresh samples revealed that the film is continuous and pinhole free. With increasing time of exposure, the film breaks apart and voids are formed. The continued growth of these voids results in the formation of separate islands (Figure S6, Supporting Information). During exposure to humidity, the grain size is significantly increased which corresponds to the observations from GIWAXS measurements. This increase is the result of mass transport from small grains to larger grains, consuming the small grains and increasing the big ones (Figure 1d).

During the SEM measurements, only little charging effects were observed even though the observed perovskite material island was not connected to each other. This indicates that the TPBi layers were not part of the mass transportation process but stayed as a continuous film that allows for electric conduction across the sample. No growth process was observed in high vacuum during SEM measurements.

3. Conclusions

LiBr has the ability to alter the surface energy of $CsPbBr_3$ in such a way that the formation of islands is preferred. We showed that this island formation process does not happen during the preparation process but rather occurs only whenever the samples are exposed to ambient air. To find the catalyst that activates the mass transport, we stored samples in various combinations of dark, bright, humid- and oxygen-free, or humid-free and oxygen-rich environments. Even after 2 weeks, only the samples exposed to ambient air showed successful island formation, which indicates that humidity activates the mass transport of island formation. When the dry air was passed through a water bubbler during the in situ GIWAXS measurements, evident changes in the diffraction rings' smoothness were observed, indicating increasing grain sizes. These findings confirm that humidity is the catalyst for the mass transport, which results in island formation of $CsPbBr_3$ perovskite material. This process increases PLQY by a factor of 350 due to suppressed exciton dissociation and a positive effect of humidity on the crystallinity. Our findings can support further research to develop high-efficiency perovskite-based LEDs and optimize process parameters during sample preparation.

4. Experimental Section

The organic material TPBi, the LiBr salt, and the $CsPbBr_3$ perovskite layers were all prepared by vacuum deposition using multisource evaporation. Prior to sample preparation, the substrates were cleaned in an ultrasonic bath for 10 min, subsequently with soapy water, distilled water, acetone, and isopropanol. Then, they were transferred into a vacuum deposition chamber (MINI PEROvap, CreaPhys GmbH, Germany). The vacuum deposition system had a cooled inner mantle to avoid re-evaporation and a temperature-stabilized substrate holder. The mantle temperature was set to −22 °C, the substrate holder was kept at room temperature and evaporation was performed at a base pressure of 10^{-6} mbar. All materials were purchased from the supplier Sigma-Aldrich and CsBr, $PbBr_2$, and LiBr were used as received, whereas TPBi was sublimed twice to increase purity.

First, 5 nm of TPBi was deposited with a rate of 0.4 Å s^{-1}, followed by 2 nm of LiBr with 0.1 Å s^{-1}. To produce $CsPbBr_3$, CsBr and $PbBr_2$ were evaporated simultaneously with rates of 0.2 and 0.23 Å s^{-1}, respectively, to ensure a stoichiometric molar ratio of 1:1. LiBr and TPBi layers were deposited with the same rates as before, following the perovskite layer again.

The PLQY measurements were performed in an integrating sphere by using the three-measurements method.[21] An OBIS LS/LX continuous wave (CW)-laser emitting at 405 nm was used as an excitation source and an Ocean Optics QW65 Pro as a spectrometer. The excitation beam had an intensity of 20 mW and was focused to a spot diameter of 870 μm. The integrating sphere was placed in ambient air (21% O_2, ≈25% H_2O) but could be purged with nitrogen, which was used to measure in an oxygen- and humidity-free atmosphere.

Cross-sections and top view SEM images were obtained with a Zeiss Gemini 500 SEM operated at 1.5 kV and observed with an Inlens detector under a 10^{-5} mbar vacuum. Before imaging, the samples were sputtered with 7 nm of a highly conductive Au:Pd alloy to avoid sample charging.

**ADVANCED
SCIENCE NEWS**

www.advancedsciencenews.com

**ADVANCED
OPTICAL
MATERIALS**

www.advopticalmat.de

Grazing-incidence wide-angle X-ray scattering (GIWAXS) measurements were conducted at beamline ID10 of the European Synchrotron Radiation Facility (ESRF) in Grenoble, France. The beam energy was 22 keV, with incidence angles of 0°–0.3°. Sample alignment was done in a nitrogen atmosphere. Before every GIWAXS measurement series, a beam damage test was performed to find the appropriate X-ray attenuators and exposure times to ensure that the samples did not suffer significant beam damage during the measurements. During the measurements, the samples were exposed to dry or humid air, while the humidity was introduced by passing the dry air through a water bubbler. GIWAXS images were acquired every 6 s during air exposure.

Supporting Information

Supporting Information is available from the Wiley Online Library or from the author.

Conflict of Interest

The authors declare no conflict of interest.

Data Availability Statement

The data that support the findings of this study are available from the corresponding author upon reasonable request.

[1] L. Schmidt-Mende, V. Dyakonov, S. Olthof, F. Ünlü, K. M. T. Lê, S. Mathur, A. D. Karabanov, D. C. Lupascu, L. M. Herz, A. Hinderhofer, F. Schreiber, A. Chernikov, D. A. Egger, O. Shargaieva, C. Cocchi, E. Unger, M. Saliba, M. M. Byranvand, M. Kroll, F. Nehm, K. Leo, A. Redinger, J. Höcker, T. Kirchartz, J. Warby, E. Gutierrez-Partida, D. Neher, M. Stolterfoht, U. Würfel, M. Unmüssig, et al., *APL Mater.* **2021**, *9*, 109202.

[2] J. Jeong, M. Kim, J. Seo, H. Lu, P. Ahlawat, A. Mishra, Y. Yang, M. A. Hope, F. T. Eickemeyer, M. Kim, Y. J. Yoon, I. W. Choi, B. P. Darwich, S. J. Choi, Y. Jo, J. H. Lee, B. Walker, S. M. Zakeeruddin, L. Emsley, U. Rothlisberger, A. Hagfeldt, D. S. Kim, M. Grätzel, J. Y. Kim, *Nature* **2021**, *592*, 381.

[3] K. O. Brinkmann, T. Becker, F. Zimmermann, C. Kreusel, T. Gahlmann, M. Theisen, T. Haeger, S. Olthof, C. Tückmantel, M. Günster, T. Maschwitz, F. Göbelsmann, C. Koch, D. Hertel, P. Caprioglio, F. Peña-Camargo, L. Perdigón-Toro, A. Al-Ashouri, L. Merten, A. Hinderhofer, L. Gomell, S. Zhang, F. Schreiber, S. Albrecht, K. Meerholz, D. Neher, M. Stolterfoht, T. Riedl, *Nature* **2022**, *604*, 280.

[4] X.-K. Liu, W. Xu, S. Bai, Y. Jin, J. Wang, R. H. Friend, F Gao, *Nat. Mater.* **2021**, *20*, 10.

[5] K. Lin, J. Xing, L. N. Quan, F. P. G. de Arquer, X. Gong, J. Lu, L. Xie, W. Zhao, D. Zhang, C. Yan, W. Li, X. Liu, Y. Lu, J. Kirman, E. H. Sargent, Q. Xiong, Z. Wei, *Nature* **2018**, *562*, 245.

[6] N. Pourdavoud, T. Haeger, A. Mayer, P. J. Cegielski, A. L. Giesecke, R. Heiderhoff, S. Olthof, S. Zaefferer, I. Shutsko, A. Henkel, D. Becker-Koch, M. Stein, M. Cehovski, O. Charfi, H.-H. Johannes, D. Rogalla, M. C. Lemme, M. Koch, Y. Vaynzof, K. Meerholz, W. Kowalsky, H.-C. Scheer, P. Görrn, T. Riedl, *Adv. Mater.* **2019**, *31*, 1903717.

[7] K. P. Goetz, A. D. Taylor, F. Paulus, Y. Vaynzof, *Adv. Funct. Mater.* **2020**, *30*, 1910004.

[8] F. Zhang, S. Huang, P. Wang, X. Chen, S. Zhao, Y. Dong, H. Zhong, *Chem. Mater.* **2017**, *29*, 3793.

[9] J.-H. Cha, J. H. Han, W. Yin, C. Park, Y. Park, T. K. Ahn, J. H. Cho, D.-Y. Jung, *J. Phys. Chem. Lett.* **2017**, *8*, 565.

[10] Z. Xiao, R. A. Kerner, L. Zhao, N. L. Tran, K. M. Lee, T.-W. Koh, G. D. Scholes, B. P. Rand, *Nat. Photonics* **2017**, *11*, 108.

[11] A. Dumont, K. Ho, H.-T. Kung, C. Qiu, P. Li, D. Luo, Y. Zhao, G. Walker, Z.-H. Lu, *Adv. Mater. Interfaces* **2020**, *7*, 2000506.

[12] Y. Vaynzof, *Adv. Energy Mater.* **2020**, *10*, 2003073.

[13] D. Di Girolamo, M. Ibrahim Dar, D. Dini, L. Gontrani, R. Caminiti, A. Mattoni, M. Graetzel, S. Meloni, *J. Mater. Chem. A* **2019**, *7*, 12292.

[14] R. Saran, A. Heuer-Jungemann, A. G. Kanaras, R. J. Curry, *Adv. Opt. Mater.* **2017**, *5*, 1700231.

[15] J. Li, L. Luo, H. Huang, C. Ma, Z. Ye, J. Zeng, *J. Phys. Chem. Lett.* **2017**, *8*, 1161.

[16] H. Fouckhardt, I. Steingoetter, M. Brinkmann, M. Hagemann, H. Zarschizky, L. Zschiedrich, *Adv. OptoElectron.* **2007**, *2007*, 27316.

[17] S. Macpherson, T. A. S. Doherty, A. J. Winchester, S. Kosar, D. N. Johnstone, Y.-H. Chiang, K. Galkowski, M. Anaya, K. Frohna, A. N. Iqbal, S. Nagane, B. Roose, Z. Andaji-Garmaroudi, K. W. P. Orr, J. E. Parker, P. A. Midgley, K. M. Dani, S. D. Stranks, *Nature* **2022**, *607*, 294.

[18] R. Guo, D. Han, W. Chen, L. Dai, K. Ji, Q. Xiong, S. Li, L. K. Reb, M. A. Scheel, S. Pratap, N. Li, S. Yin, T. Xiao, S. Liang, A. L. Oechsle, C. L. Weindl, M. Schwartzkopf, H. Ebert, P. Gao, K. Wang, M. Yuan, N. C. Greenham, S. D. Stranks, S. V. Roth, R. H. Friend, P. Müller-Buschbaum, *Nat. Energy* **2021**, *6*, 977.

[19] A. Greco, A. Hinderhofer, M. I. Dar, N. Arora, J. Hagenlocher, A. Chumakov, M. Grätzel, F Schreiber, *J. Phys. Chem. Lett.* **2018**, *9*, 6750.

[20] N. Mrkyvkova, V. Held, P. Nádaždy, R. Subair, E. Majkova, M. Jergel, A. Vlk, M. Ledinsky, M. Kotlár, J. Tian, P. Siffalovic, *J. Phys. Chem. Lett.* **2021**, *12*, 10156.

[21] J. C. de Mello, H. F. Wittmann, R. H. Friend, *Adv. Mater.* **1997**, *9*, 230.